Langmuir

ARTICLE

pubs.acs.org/Langmuir

Single Vesicle Observations of the Cardiolipin−Cytochrome *c* Interaction: Induction of Membrane Morphology Changes

Paul A. Beales,[†,§] Chris L. Bergstrom,[‡] Nienke Geerts,[†] John T. Groves,[*,‡] and T. Kyle Vanderlick[*,†]

[†]Department of Chemical and Environmental Engineering, Yale University, New Haven, Connecticut 06511, United States

[‡]Department of Chemistry, Princeton University, Princeton, New Jersey 08544, United States

Supporting Information

ABSTRACT: We present a novel platform for investigating the composition-specific interactions of proteins (or other biologically relevant molecules) with model membranes composed of compositionally distinct domains. We focus on the interaction between a mitochondrial-specific lipid, cardiolipin (CL), and a peripheral membrane protein, cytochrome *c* (cyt *c*). We engineer vesicles with compositions such that they phase separate into coexisting liquid phases and the lipid of interest, CL, preferentially localizes into one of the domains (the liquid disordered (L_d) phase). The presence of CL-rich and CL-depleted domains within the same vesicle provides a built-in control experiment to simultaneously observe the behavior of two membrane compositions under identical conditions. We find that cyt *c* binds strongly to CL-rich domains and observe fascinating morphological transitions within these regions of membrane. CL-rich domains start to form small buds and eventually fold up into a collapsed state. We also observe that cyt *c* can induce a strong attraction between the CL-rich domains of adjacent vesicles as demonstrated by the development of large osculating regions between these domains. Qualitatively similar behavior is observed when other polycationic proteins or polymers of a similar size and net charge are used instead of cyt *c*. We argue that these striking phenomena can be simply understood by consideration of colloidal forces between the protein and the membrane. We discuss the possible biological implications of our observations in relation to the structure and function of mitochondria.

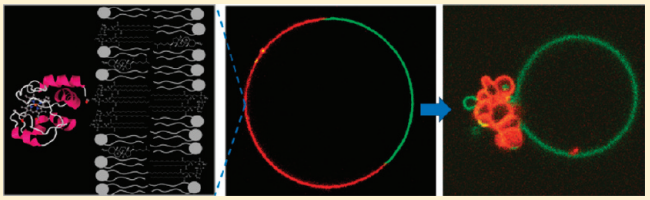

INTRODUCTION

Simple biomolecular systems consisting of only a few components are useful tools to elucidate the fundamental interactions and behaviors of the constituent species in a way that is inaccessible when studying complex whole cells or living organisms. For example, synthetic lipid vesicles composed of a minimal number of lipid constituents are commonly used as model systems for biomembranes. Giant unilamellar lipid vesicles (GUVs), several micrometers in diameter, are large enough for their details to be individually resolved by light microscopy techniques. This feature permits observation of single vesicles with high spatial resolution, allowing the temporal evolution of morphological transformations of the membrane to be monitored. Direct observation has compelling advantages over experiments on samples of submicroscopic vesicles that, while yielding information on the ensemble average behavior with high statistics, offer no information about the distribution of the properties of interest and lack sensitivity to rare events.

In this study, we develop heterogeneous GUVs with spatially localized domains enriched in the lipid of interest such that the differential response of disparate membrane compositions can be observed under identical conditions in response to the additional of external stimuli, in this case, a protein. We choose to focus on the interactions of the peripheral membrane protein cytochrome *c* (cyt *c*) with the lipid cardiolipin (CL), both being important constituents of mitochondria.

Mitochondria are cellular organelles that, according to the endosymbiotic theory,[1] originated as separate prokaryotic organisms. They are perhaps best known as the energy producing centers of the eukaryotic cell (via ATP production by aerobic respiration), but are also involved in many other functions, including cell death through a pathway known as apoptosis. Mitochondrial dysfunction is linked to many diseases,[2] including myopathy, diabetes, and neurological disorders.

The structure and organization of mitochondria have been elucidated in great detail by electron microscopy techniques.[3] The mitochondria are enclosed by a double membrane structure. The outer mitochondrial membrane has a lipid composition similar to that of the plasma membrane, whereas the inner membrane is rich in an unusual lipid: CL. CL has four unsaturated acyl chains (as opposed to the usual two) and is found almost exclusively in the membranes of mitochondria or prokaryotes.[4] The inner mitochondrial membrane has a larger surface area than does the outer membrane and folds into invaginations called cristae. The intermembrane space has high concentrations (estimated to be in the range 0.5−5 mM[5]) of the heme protein cyt *c*, the physiological roles of which include transport of electrons between complex III and

Received: December 10, 2010
Revised: March 29, 2011
Published: April 19, 2011

complex IV of the electron transport chain. Further, cyt *c* is a critical signaling molecule that leads to activation of caspase enzymes in the intrinsic pathway of cellular apoptosis upon mitochondrial outer membrane permeablization.[6]

The interactions between CL and cyt *c* are considered to play an important role in both respiration and apoptosis. The inner mitochondrial membrane contains approximately 18% by weight CL as compared to only about 4% in the outer membrane.[7] Cyt *c* is polycationic (estimated net molecular charge +9*e* at pH 7.4[8]) and is readily soluble in water, but interacts strongly with anionic CL in the inner mitochondrial membrane, initially through electrostatic attraction. One of the hydrocarbon tails of CL is then thought to insert into the structure of cyt *c*, augmenting its electrostatic association by the addition of a hydrophobic interaction.[9] There is evidence for conformational changes in the protein upon this type of hydrophobic anchoring to CL-containing membranes[10,11] that alter the redox potential and reactivity of the heme group[12,13] and may be important in cyt *c*'s role in the electron transfer chain. Peroxidation of CL catalyzed by CL-bound cyt *c* is suggested as a step preceding the release of cyt *c* in apoptosis.[14] Escape of cyt *c* into the cytosol during apoptosis is accompanied by observable morphology changes in the inner mitochondrial membrane (mitochondrial cristae remodelling):[15] the narrow folded structures of the cristae of healthy mitochondria are seen to swell, eventually forming many vesicular compartments within the mitochondrial matrix. Recently, specific targeting of CL−cyt *c* complexes has been proposed as a new strategy for development of antiapoptotic drugs.[16]

In this Article, we describe our investigations of the interaction of cyt *c* with laterally heterogeneous GUVs containing physiologically relevant compositions of CL using laser scanning confocal fluorescence microscopy. Confocal microscopy provides thin optical sections that allow clear, simultaneous observation of the vesicle membranes and their internal and external aqueous environments. We have observed remarkable morphological transitions in the CL-containing portions of the membrane that are triggered by the cyt *c*−CL interaction. These intrinsic protein−membrane properties may be relevant to the formation of folded cristae structures in the inner mitochondrial membrane and membrane morphology changes observed during apoptosis.

MATERIALS AND METHODS

Materials and Protein Labeling. The lipids 1,2-dioleoyl-*sn*-glycero-3-phosphocholine (DOPC), 1,2-dipalmitoyl-*sn*-glycero-3-phosphocholine (DPPC), cardiolipin (heart, bovine-disodium salt) (CL), and cholesterol (chol) were purchased from Avanti Polar Lipids (Alabaster, AL). The fluorophore-labeled lipids *N*-(7-nitrobenz-2-oxa-1,3-diazol-4-yl)-1,2-dihexadecanoyl-*sn*-glycero-3-phosphoethanolamine, triethylammonium salt (NBD-PE), Lissamine rhodamine B 1,2-dihexadecanoyl-*sn*-glycero-3-phosphoethanolamine, and triethylammonium salt (Rh-PE) were purchased from Invitrogen Molecular Probes. Yeast cyt *c* fluorescent labels and aminodextran were also from Invitrogen. α-Synuclein protein was obtained from rPeptide. TCEP was from Fluka. All other reagents and proteins (horse heart cyt *c*, yeast (*S. cerevisiae*) cyt *c*, horse heart myoglobin, chicken egg white lysozyme, 25 kDa branched polyethylenimine (PEI), and PAMAM dendrimers (generations 3 and 4) with an ethylenediamine core) were obtained from Sigma Aldrich. Yeast cyt *c* was labeled at Cys102 with maleimide dyes[17] (Alexa Fluor 633 C5 maleimide and Alexa Fluor 568 C5 maleimide) according to manufacturer protocol and was separated from excess unreacted dye on a DEAE Sephadex column. Mass spectrometry results show ∼5% of cyt c singly labeled with the Alexa Fluor 633 dye, and >50% singly labeled with the AlexaFluor 568 dye, with no evidence of any multiply labeled protein in either case. No other proteins or polymers, besides the yeast cyt *c*, were labeled with fluorophores for this study.

Vesicle Formation. Giant unilamellar vesicles (GUVs) were formed by electroformation. Lipid stock solutions in chloroform were made up at the desired molar ratio to a total lipid concentration of 1.0 mM. 20−50 μL of lipid in chloroform solution was placed dropwise onto the platinum wires of the electroformation chamber and dried under vacuum for at least 4 h. For formation of phase-separated GUVs, a preheated 300 mM aqueous sucrose solution was added to the electroformation chamber in an oven at a temperature in excess of 50 °C such that all lipids were in the fluid phase. (Note for experiments conducted at 390 mM NaCl and 780 mM NaCl, 1.0 and 2.0 M sucrose solutions were used, respectively, to ensure no significant osmotic stress across the membranes during experiments.) A 3.0 V a.c. (or 1.0 V a.c. for mixtures containing anionic lipids) electric field was applied across the platinum wires at 10 Hz for 30 min, 3.0 Hz for 15 min, 1.0 Hz for 7 min, and 0.5 Hz for 7 min. The vesicles were then removed from the chamber and allowed to slowly cool to room temperature. GUVs composed entirely of lipids with melting temperatures below ambient laboratory temperature were formed by the same protocol except at room temperature.

Confocal Microscopy. Vesicle samples were imaged using the Leica TCS SP5 confocal system. The objective lens used was a Leica 63×/1.3 N.A. Plan Apo DIC glycerin immersion lens. The Rh-DPPE and Alexa Fluor 568 probes were excited by a DPSS laser at 561 nm, the NBD-PE probe was excited with the 488 nm line of an argon laser, and the Alexa Fluor 633 was excited with the 633 nm line of a helium neon laser.

Glass bottom culture dishes (MatTek Corp., part no. P35G-1.5-20-C) were treated with a 10% bovine serum albumin (Sigma) solution prior to use to prevent the vesicles from adhering to the glass coverslip. 25−50 μL of prepared vesicle solution and 50 μL of microscope buffer (10 mM HEPES pH 7.4, adjusted to 336 mOsm with NaCl) were deposited on the glass slide and incubated ∼15 min to allow vesicles to settle to the bottom of the sample. (Note that for the experiments conducted at differing ionic strengths, the external media were either 330 mM glucose, or 10 mM HEPES (pH 7.4) with 545 mM NaCl, or 10 mM HEPES (pH 7.4) with 1095 mM NaCl.) All vesicle samples had been cooled to room temperature for several hours to allow phase separation and domain ripening to proceed to conclusion. With the vesicles now in a single focal plane, the microscope was used to check that an adequate number of vesicles were present.

All proteins and polymers to be added to the vesicles solution were dissolved or diluted into the microscope buffer, and then proteins were dialyzed against the same buffer to remove salts or other contaminants using D-Tube Dialyzers MWCO 6−8 kDa from Calbiochem or Slide-A-Lyzer Mini Dialysis Units 3500 MWCO from Pierce. A stock solution of the protein/polymer (to result in 17 μM final diluted concentration) was added carefully to the top of the sample drop. The protein/polymer solutions were always added to the vesicles once they had phase separated and were at room temperature. Samples were monitored for at least 30 min in every case. All images are taken at room temperature (21 ± 2 °C).

RESULTS

Our findings show that yeast cyt *c* binds to CL-containing membranes but not to neutral DOPC-containing membranes. Figure 1A shows a giant DOPC vesicle labeled with NBD-PE (green) cohabiting with unlabeled 4:1 DOPC:CL GUVs. This mixed population of vesicles resides in the presence of Alexa Fluor 568 labeled yeast cyt *c* (red). The images from the individual channels and the composite image clearly show that cyt *c* binds strongly to the CL-containing vesicle membranes, as indicated by the red fluorescence of those vesicles, with no detectable binding of the cyt *c* to the DOPC-only membranes.

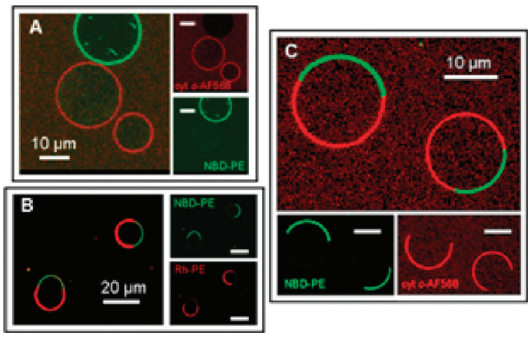

Figure 1. (A) DOPC vesicles labeled with NBD-PE (green) coexisting with 4:1 DOPC:CL vesicles (unlabeled) and Alexa Fluor 568 labeled cyt *c* (red). The cyt *c* only binds detectably to the CL-containing vesicles. (B) Phase-separated vesicles containing 10% CL, 25% chol, 27.5% DOPC, 37.5% DPPC (0.5% Rh-PE, 0.5% NBD-PE). The Rh-PE (red) labels the L_d phase, and the NBD-PE (green) labels the L_o phase. (C) Phase-separated CL-containing vesicles labeled only with the NBD-PE lipid probe (green) in solution with Alexa Fluor 568 labeled cyt *c* (red). The cyt *c* only binds detectably to the CL-containing L_d domains. The insets represent the separate red and green fluorescence channels that are collected and superimposed to create the composite image.

We engineer asymmetric distributions of CL within the membrane of single vesicles by incorporating CL into lipid mixtures that are known to phase separate into two distinct liquid phases: ternary mixtures of DOPC/DPPC/cholesterol have a large region of their phase diagram wherein these membranes demix to form liquid-ordered (L_o) and liquid-disordered (L_d) domains.[18] The L_d phase of these model membranes is rich in DOPC due to its unsaturated hydrocarbon tails, which do not favor packing into more ordered phases, and the L_o phase is rich in the saturated DPPC. Cholesterol partitions into both phases but is slightly enriched in the L_o domains as compared to the L_d phase. GUVs composed of 37.5:37.5:25 DOPC:DPPC:cholesterol at 22 °C are within this region of liquid−liquid phase separation; domains of these two liquid phases coalesce and ripen to form two large domains on the vesicle surface, one of each phase. We exchanged 10 mol % DOPC for 10 mol % CL based upon two assumptions: that CL, due to its high degree of chain unsaturation, will also prefer to partition into the L_d phase, and that despite such a significant change in lipid composition, the membrane will still be in a region of phase space for liquid−liquid phase coexistence. This indeed turned out to be the case: Figure 1B shows GUVs composed of 10% CL, 25% cholesterol, 27.5% DOPC, and 37.5% DPPC labeled with 0.5% Rh-PE and 0.5% NBD-PE. The Rh-PE (red) probe is known to preferentially partition into the L_d phase and NBD-PE (green) into the L_o phase.[19] The evolution of phase separation and domain ripening proceeds in a fashion similar to liquid−liquid phase separation in the DOPC/DPPC/cholesterol system. Domain boundaries visibly fluctuate during the time of the observations, indicative of their fluidic nature. The domains are observed to coalesce over several minutes, minimizing the line tension between phases, until the GUV consists of two domains, one of each phase.

Yeast cyt *c* binds preferentially to regions of the membrane that are rich in CL. Figure 1C demonstrates GUVs of the same composition as Figure 1B except that the vesicles do not contain the Rh-PE lipid probe, leaving the L_d domains unlabeled. Alexa Fluor 568 labeled yeast cyt *c* (red) is added to this sample and can only be detected to bind to the L_d domains into which the CL has partitioned.

The CL-containing domain is observed to undergo a dramatic morphological transition upon addition of yeast cyt *c* to phase-separated GUVs with CL-rich domains. Initially, sections of the L_d domain appear to form bright beads on the membrane, Figure 2A. These beads can often be resolved as membrane buds that bulge out from the vesicle. Therefore, we will assume that all of the protein−lipid complexes that appear as beads on the membrane are buds where in many cases the structural details of the budded membranes are on too short a length scale to be easily resolved under optical resolution. These buds grow in size and aggregate together as the CL-rich domain folds up on itself. The folded structure of collapsed domains can be seen in Figure 2B−D. The collapsed domains exhibit a variety of forms, including extended wispy structures (Figure 2E) and tightly folded domains (Figure 2F), indicative of a nonequilibrium structure to their final morphologies. The domains on the vesicle in Figure 2F collapsed before they had ripened into a single domain, with two large CL-rich domains coexisting that independently collapsed into tight, folded structures. The collapse of the L_d domains on these vesicles was reproducible and widespread throughout the samples as shown in Figure 2G, where white arrows indicate collapsed domains on different vesicles.

The initiation of domain collapse was always preceded or accompanied by cyt *c* leakage, at least partial and usually complete, into the interior volume of the vesicle. This can be seen in Figure 2F where the yeast cyt *c* is labeled with Alexa Fluor 633 (blue): a fluorescent signal is observed inside the vesicle in this image section through the vesicle equator, ∼49% of the intensity of the cyt *c* concentration in the external medium (note also that in Figure 1C the GUVs have leaked ∼99% (left) and ∼97% (right) to the cyt *c*). Those vesicles that had not fully leaked before collapse occurred leaked during the final processes of collapse to a compact state. This permeability of the membrane is perhaps indicative of the formation of defects in the membrane during the domain collapse process. This membrane permeability would aid the necessary internal volume change that occurs as a result of the collapse, allowing ions and small macromolecules in solution to exchange across the membrane such that a large osmotic pressure difference is not created between the internal and external aqueous pools of the vesicle. This accommodation to the change in volume could also explain why, over all experiments, domain budding to the outside of vesicles is noticeably more prevalent (>80% of cases).

The time-scales observed for the initiation of beading after cyt *c* addition and for complete collapse varied widely, even between neighboring GUVs within the same sample. Time-lapse videos of domain collapse in single vesicles from an initial state of domain beading were obtained at a rate of approximately one frame every 2.5 s (e.g., see Supporting Information videos S1, S2). The initial beading of the CL-rich domains was observed to begin from between ∼2−30 min after the addition of cyt *c*. Once beading began, initiation of complete collapse of the domain to its final folded structure was seen to take anything from 10 s to >10 min. Furthermore, this final stage of collapse itself, from the initial few beads to the collapsed state, could be rapid (a few seconds) or relatively slow (a few minutes). This range of time scales for the kinetics of morphological changes from vesicle to vesicle observed within the same sample is further indication of a nonequilibrium, aggregation-like transition in the morphology of the L_d domains. It also indicates an activated process where an energy barrier likely exists between the "pre-bud" and "post-bud" states.

Time series images of single vesicle morphology changes are shown in Figure 3. Only selected images are shown during each

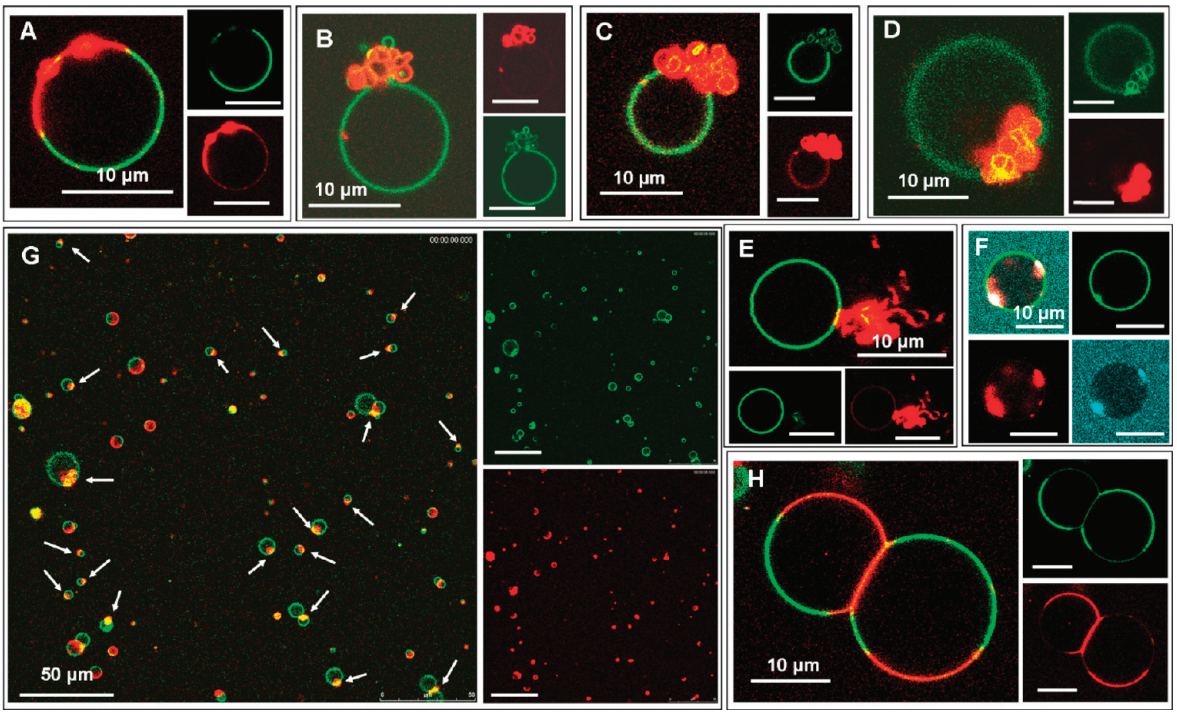

Figure 2. All vesicles are phase-separated CL-containing GUVs labeled by the NBD-PE (green) and Rh-PE (red) probes. Images A−E, G, and H are GUVs interacting with Alexa Fluor 568 cyt *c* (red), and image F is a GUV in the presence of Alexa Fluor 633 labeled cyt *c* (blue). (A) Beading of the membrane can be observed in the L_d domain. (B−D) The L_d domains on the vesicles have collapsed into a folded structure where the folds of the membrane are resolvable under the confocal microscope. (E) The morphology of the L_d domain after cyt *c*-induced collapse appears to have a "wispy" morphology. (F) Two separate L_d domains coexisting in the same vesicle have collapsed into tight, folded structures. (G) Lower magnification image of many GUVs in the sample. White arrows indicate L_d domains that have collapsed to a folded structure after the addition of cyt *c*, thus demonstrating that the morphological transition we observe represents the majority behavior of vesicles in the sample. (H) Strong adhesion between the negatively charged, CL-containing L_d domains induced by the polycationic cyt *c* results in membrane deformation and a large osculating area between the two GUVs. The insets represent the separate fluorescence channels that are collected and superimposed to create the composite image.

time-lapse image series. The time origin noted for both of these vesicles is the time at which the first image of each vesicle was collected, rather than the time at which cyt *c* was added to the sample. Vesicle A was monitored for approximately 11 min before complete collapse had finished. The "beads" or buds in the membrane can be seen to appear and disappear from the plane of view due to diffusion around the vesicle surface. In some images (∼10%), the budded nature of the membrane can be resolved, for example, after 94, 203, 332, and 512 s, as demonstrated by the magnified vesicles insets in Figure 3. However, in many cases, the structure of these buds cannot be clearly distinguished, likely due to their structural details being of length scales below that of the optical resolution. Note that there is rotational diffusion of the vesicle and/or the domain boundaries during imaging such that the relative locations of the L_d and L_o phases move between images. The L_o domain does not undergo any detectable changes during collapse of the L_d phase (except for the necessary small increase in curvature as the vesicle decreases in size). The NBD-PE dye labeling the L_o phase photobleaches and becomes fainter during the time-lapse imaging; therefore, a green dotted line is used to highlight the location of the L_o domain in the final image to aid the reader's eye. A significant decrease in vesicle size can be seen between the initial and final images of this series due to the collapse of the domain. On scanning through vesicles in the *z* direction after complete domain collapse, no evidence of uncollapsed portions of L_d membrane was observed. Vesicle B shows the latter stages of domain collapse on a vesicle. Two large L_d membrane "beads" can already be detected in the image plane of the initial image with full collapse from this state occurring over a period of approximately 2 min. Again, no morphological changes are detected in the L_o domain.

The behavior of the CL-rich domains of these vesicles was observed after the addition of several other proteins and polymers in an attempt to elucidate which properties of the yeast cyt *c* are important in inducing the collapse. The alternatives used were horse heart cyt *c*, α-synuclein, horse heart myoglobin, chicken egg white lysozyme, 25 kDa branched PEI, 10 kDa aminodextran, and generations 3 and 4 PAMAM dendrimers terminated in amine groups. Myoglobin is a relatively small heme protein (17.6 kDa) with no net charge. Lysozyme is a globular protein with a size (14.3 kDa) and net charge (+8*e* at pH 7.4[20]) similar to those of cyt *c*. α-Synuclein is a natively unstructured 14.5 kDa protein that is known to interact with membranes containing negatively charged headgroups;[21] although it has a net charge of −9*e*, its N-terminal region is rich in positively charged residues. The cationic polymers used were aminodextran polymer (M_w of 10 kDa and an average of 5.7 amines per polymer), 25 kDa branched PEI, and two PAMAM dendrimers: generation 3 (M_w of 6909 kDa and 32 surface amine groups) and generation 4 (M_w of 14 215 kDa and 64 surface amine groups).

The addition of horse heart cyt *c*, lysozyme, 25 kDa branched PEI, and both genrations 3 and 4 PAMAM dendrimers also similarly induced collapse of the CL-rich L_d domains, whereas the other tested additives did not (Figures 4 and S1). Electrostatic binding of linear polymers and copolymers to oppositely charged membranes (sometimes resulting in electroneutrality)

dx.doi.org/10.1021/la104924c |*Langmuir* 2011, 27, 6107–6115

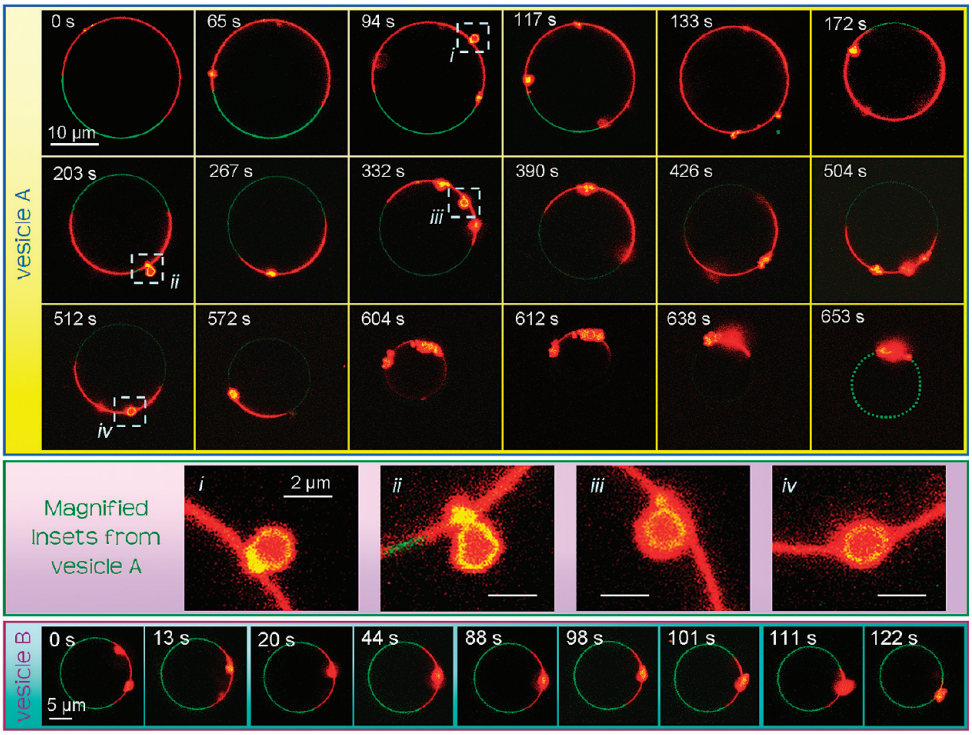

Figure 3. Time-lapse images of two vesicles during domain collapse. The CL-containing GUVs are labeled with the NBD-PE (green) and Rh-PE (red) probes. The origin for the time scale for each vesicle is from the start of observation of the vesicle and not the time cyt *c* was added to the samples. The NBD-PE dye photobleaches during the time-lapse imaging: a green dotted line is drawn in the final image of vesicle A to highlight the location of the L_o domain. Vesicle A is monitored over a period of approximately 11 min, and vesicle B is monitored over a period of approximately 2 min. Insets i−iv show magnified sections of vesicle A's membrane where the budded structure within the L_d domains can be clearly resolved.

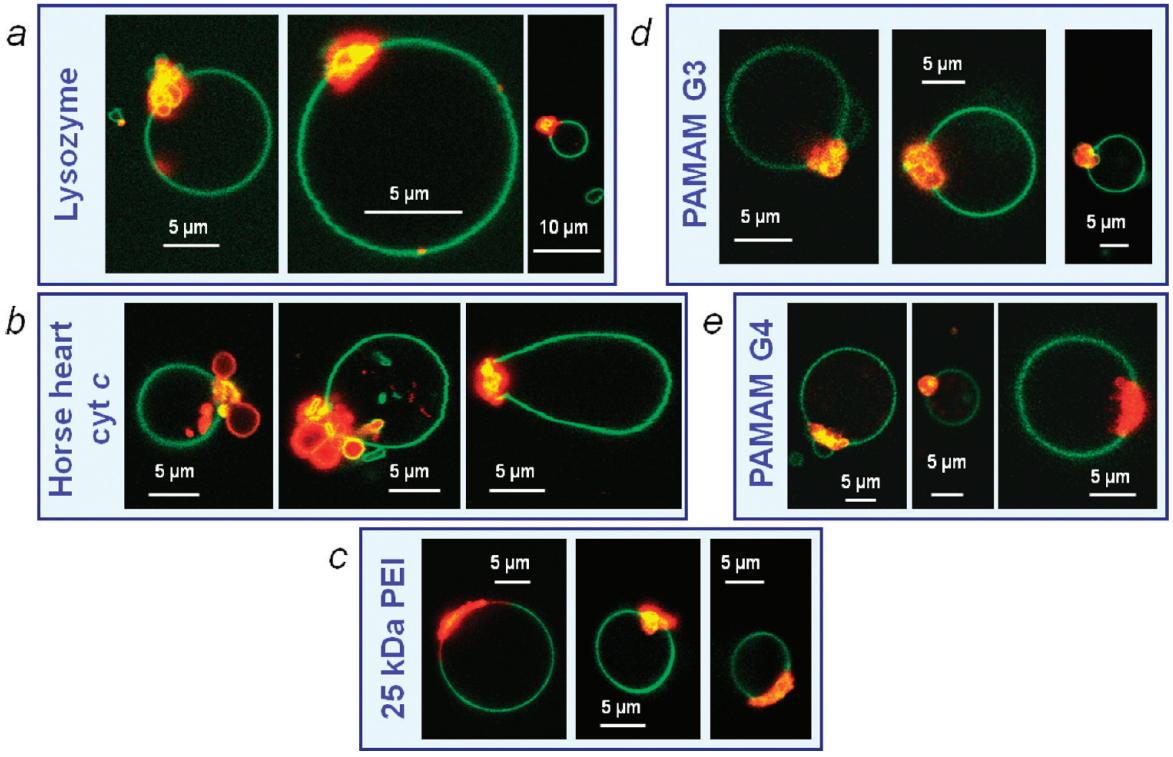

Figure 4. Resultant vesicle morphologies of phase-separated, CL-containing GUVs after incubation in solution with (a) lysozyme, (b) horse heart cyt *c*, (c) 25 kDa branched PEI, (d) generation 3 PAMAM dendrimer, and (e) generation 4 PAMAM dendrimer. Rh-DPPE (red) labels L_d domains, and NBD-PE (green) labels the L_o domains.

dx.doi.org/10.1021/la104924c |*Langmuir* 2011, 27, 6107–6115

has previously been reported;[22,23] however, observation of such morphology changes induced by polycationic dendritic or branched polymers is, to our knowledge, a new phenomenon. (Note that the PAMAM dendrimers, most prevalently generation 3, sometimes caused the membrane folds to bud off from the CL-rich domain into the vesicle interior: see Supporting Information video S3.) This implies that the observed phenomena are not specific to the structure of cyt *c* and that other molecules of similar size and net charge can induce the similar behavior. This suggests a nonspecific electrostatic origin for the domain folding and collapse. It is interesting to note that the aminodextran did not induce this behavior despite being a similar molecular weight to cyt *c* and possessing a polycationic net charge. This could be due to the lower net positive charge on the aminodextran and also the lack of a definite globular tertiary structure of this polymer, because the branched and dendritic synthetic polymers tested, which, due to polymer branching, would retain a more globular shape upon binding to the membrane, also resulted in the collapse of the CL-rich domains.

To investigate the role of electrostatic interactions in the observed morphology transitions, we conducted experiments over a range of ionic strengths (Figure S2). Our previous experiments were all in an aqueous media with a final ionic strength of 100 mM NaCl. At very low ionic strength (0 mM NaCl: obtained using a 330 mM glucose solution as the incubation media), qualitatively similar morphology changes were observed in the L_d domains. However, at higher ionic strengths (390 and 780 mM NaCl), the normal, unperturbed morphology of the phase-separated GUVs was still observed after 30 min incubation with 17 μM cyt *c*. This high ionic strength cut off of the L_d domain budding and collapse suggests a role for electrostatic interactions in the mechanisms of these phenomena. At higher ionic strengths, the increased ion concentration screens electrical charges, reducing the magnitude and range of electrostatic interactions.

Addition of cyt *c* to a sample of CL-containing vesicles induces attraction between the CL-containing domains of neighboring vesicles. This is exemplified in Figure 2H where two CL-containing L_d domains (red) on adjacent vesicles are adhering strongly as seen by their large osculating region and membrane deformation from their native spherical geometries. Cyt *c* was not seen to induce attraction between samples of DOPC vesicles, and adhesion was not observed between the CL-deprived L_o domains of neighboring phase-separated vesicles. Therefore, this attraction between membranes is specific to regions containing cyt *c* bound to CL lipids; this excludes the possibility of the adhesion between the vesicles being caused by an osmotic depletion force[24] induced by free cyt *c* molecules in the surrounding solution, which would not be specific to lipid composition. This adhesion between anionic CL-containing membranes induced by polycationic cyt *c* is consistent with many reports of adhesion of charged membranes induced by oppositely charged polyelectrolytes, for example, cationic lipid membranes complexing with DNA.[25] This is due to a short-range interaction induced between the normally repulsive lipid membranes by the polyion.[26] This observation is also in agreement with a report of electrostatically driven aggregation of anionic DMPG liposomes induced by addition of cyt *c*.[27] Indeed, the folding and collapse of the L_d domains induced by cyt *c* was also observed in phase-separated GUVs where the anionic lipid DOPG had been substituted for CL (Figure 5), thus lending further support to the interpretation that the driving force behind the morphological changes is nonspecific and electrostatic in origin. Cyt *c* induced attraction between anionic lipid membranes might not only be significant for intermembrane adhesion between opposing vesicles but could also be significant for intramembrane interactions between segments of membrane in the same vesicle as well as be significant to the structure and function of natural mitochondria. Both of these possibilities will be discussed in more detail below.

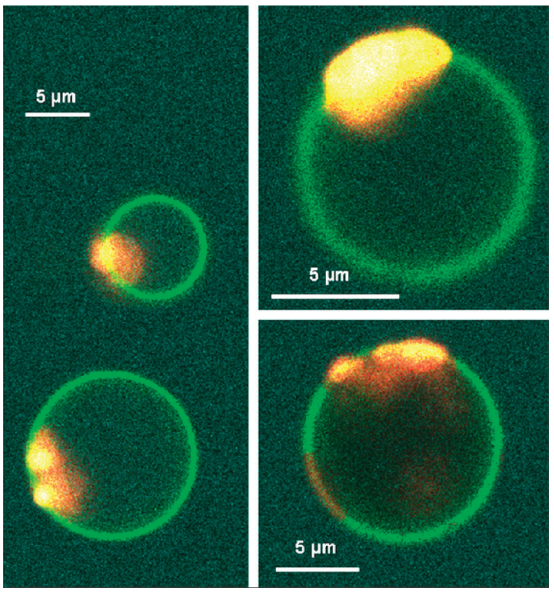

Figure 5. Alexa Fluor 633-labeled yeast cyt *c* (blue) induces the collapse of L_d domains in liquid−liquid phase-separated GUVs containing 10 mol % DOPG. Rh-DPPE (red) labels L_d domains, and NBD-PE (green) labels the L_o domains.

DISCUSSION

We have found that dramatic morphology changes can be induced in CL-containing membranes when they are perturbed by the presence of cyt *c*. Cyt *c* is observed to bind specifically to CL-containing domains in phase-separated GUVs. The CL-rich domains are seen to initially undergo budding, which is followed by a collapse of these membranes into a folded state. Qualitatively similar phenomena can also be induced in these membranes by addition of proteins or polymers with a similar size and net charge to cyt *c*. Cyt *c* was also observed to induce these phenomena in membranes where CL was substituted for another anionic lipid, DOPG. Strong attraction is induced by cyt *c* between the apposing CL-rich domains of neighboring GUVs. However, the budding and collapse phenomena ceased to be observed at elevated ionic strengths. All taken together, these reported observations indicate a significant role for electrostatic interactions in driving these morphology transitions. Below we will provide an argument in support of our proposed physical mechanism that drives these morphological phenomena, and we will also discuss their possible biological implications.

Proposed Physical Mechanisms. Transformations in membrane morphology induced by proteins are a delicate negotiation between the interactions, mechanical properties, and molecular geometries of the constituent species.[28] A variety of proteins, peptides, and modified lipids are known to form membrane structural changes including budding by inducing positive or negative curvature stress.[29,30] Among these are dynamin and the apoptotic proteins tBid and BAX. Below we will tentatively describe our hypotheses for the underlying physical interactions and processes that drive the folding of CL-containing portions of

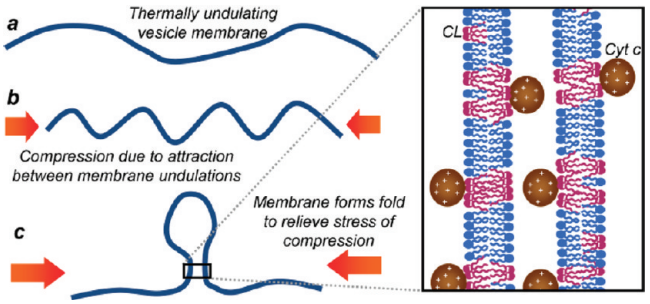

Figure 6. Proposed model for the mechanism of domain collapse. A compressive, electrostatic force is exerted on the CL-containing membrane by the cyt *c* molecules. The positively charged cyt *c* resides within the undulations of the thermal fluctuations of the negatively charged membrane, attracting nearby portions of membrane toward one another. This causes compression of the membrane ripples, increasing the curvature stress in the membrane. This stress is released by formation of a single localized fold in the membrane. Compare the beading of the membrane that we observe with reports of a ripple to fold transition during the compression of thin films.[35]

membrane induced by bound cyt *c*. These mechanisms rely on nonspecific physical interactions between the protein and the membrane, which is considered as a charged particle interacting with a thin, soft membrane of the opposite charge. Therefore, we argue that the phenomena we report here can, in general, be understood without appealing to the added complexity of the fine details of protein chemistry and secondary structure, but instead rely on colloidal interactions of proteins with the interfacial membrane surface.

The observed membrane morphological changes are not likely to be due to an induced area difference by cyt *c* binding to one monolayer of the lipid bilayer. If a protein binds only to one monolayer of the bilayer, it can increase the area of one monolayer with respect to the other, causing the bilayer to bend in an attempt to compensate.[28] In our experiments, many vesicles were observed to have leaked before collapse of the L_d domains occurred. Accordingly, cyt *c* can bind to both the inner and the outer leaflets of the membrane, and we conclude that no significant area difference exists between the monolayers that might drive morphological changes.

Despite the vesicle membrane appearing to have a smooth spherical shape before domain collapse transpires, thermally driven undulations occur within the soft lipid membrane on length scales below the resolution of optical microscopy.[31] The mean-squared displacement, $\langle h^2 \rangle$, of a membrane of area A, under vanishing tension, from its spherical geometry driven by these fluctuations can be estimated by integrating over all possible modes of oscillation to obtain the expression $\langle h^2 \rangle \approx k_B T A/(4\pi^3 \kappa_b)$,[32] where $k_B T$ is a measure of the thermal energy of the system and κ_b is the elastic bending modulus of the membrane, which we will approximate as 10 $k_B T$.[33] Therefore, the rms displacement of the membrane of a 10 μm diameter vesicle from its spherical shape is approximately $(\langle h^2 \rangle)^{1/2} \approx 500$ nm. This value is consistent with our observation that the GUVs maintain their spherical shape with small membrane fluctuations visible microscopically. However, the presence of membrane fluctuations of this magnitude would lead to membrane-bound cyt *c* molecules residing between sections of CL-rich membrane as shown in Figure 6. Because we have already demonstrated that cyt *c* induces attraction between the anionic domains of opposing vesicles, we infer that the cyt *c* could also induce attraction between segments of the same membrane placed in apposition via these thermal fluctuations.

Our proposed mechanism for the cyt *c*-induced collapse behavior of the CL-rich domains is a consequence of induced attraction between entropically driven undulations that create apposing membrane segments of the same domain. Theoretical studies have predicted that attraction between segments of the same membrane within a vesicle can lead to a transition between an inflated structure and a compact, folded, crumpled morphology.[34] The short-range electrostatic attraction that cyt *c* induces between anionic membranes may induce a lateral compressive force acting on the membrane. Pocivavsek et al. have shown that lateral compression of thin elastic films can result in a transition between ripples and folds.[35] In the cyt *c*−GUV system we study here, we propose that the ripples represent the entropic, thermal fluctuations and the folds are analogous to buds/beads that appear in the membrane in the initial stages of domain collapse. As the fluctuating membrane is compressed due to the stress of attraction between segments of the bilayer, the undulations initially condense and thereby increase the overall curvature of the membrane domain. This increase in curvature elastic stress in the membrane caused by the compression is then released into a highly localized fold (i.e., the membrane buckles), allowing other parts of the membrane to relax to a more gently rippled state (see Figure 6). Our experimental observations provide strong evidence for the formation of these folds within the membrane as they occur on optically resolvable length scales. The CL-rich L_d domain then proceeds to fold up further due to cyt *c*-induced electrostatic attraction between coexisting membrane buds and between membrane buds and other portions of the L_d domain. A lateral compression on the membrane is a more plausible explanation than a mechanism by which cyt *c* induces a lateral tension in the membrane because such a tension would oppose the crumpling and collapse of the domains that we observe experimentally.

The increased membrane curvature required for folding may be aided by clustering of CL lipids induced by cyt *c* binding to the membrane.[36,37] Cyt *c* binding to the CL-containing domains may induce electrostatic clustering of CL lipids into nanoscopic membrane domains[38] that prefer a negative spontaneous curvature (i.e., monolayers that prefer to bend toward the aqueous phase), thereby inducing the bilayer to bend and reducing the energy cost for membrane bending due to the lateral electrostatic compression induced by cyt *c* on the membrane. Furthermore, the presence of cholesterol, which is known to also prefer a negative spontaneous curvature,[39] could assist in this bending. In the extreme of membranes with very high CL compositions, charge neutralization of the CL headgroup by low pH, high concentrations of monovalent ions, or cyt *c* is known to induce formation of an inverted hexagonal (H_{II}) phase,[40,41] a phase preferred by lipids that desire a negative monolayer spontaneous curvature. However, it should be noted here that we do not believe that the domain collapse we observe in these GUVs is due to a transition between a L_d bilayer phase and an inverted H_{II} phase induced by addition of cyt *c* because our vesicles have a relatively low (near physiological) CL composition, and, in many of our images, we can resolve a folded structure of the membrane in the collapsed domain that is not consistent with the formation of a H_{II} phase, for example, Figure 2B−D. However, by optical microscopy alone, it is difficult to completely rule out the possibility of small, locally stable H_{II} domains contributing in the folding transitions we observe in the CL-rich domains.

While we clearly show that these morphology transitions driven by a range of polycationic polymers and proteins are primarily driven by electrostatic processes, there will be quantitative details between the morphology transitions induced by these different perturbants. For example, here we have found that

the linear, cationic aminodextran we investigate cannot induce the same morphology changes as the dendritic and branched polymers or the globular proteins; therefore, polymer shape and shape stability upon adsorption to the membrane are clearly important. Also, we note in the case of the PAMAM G3 dendrimer that the dendrimer-induced folds in the membrane can sometimes bud off into the lumen of the GUV. Absorption of linear polymers to membranes by hydrophobic and/or electrostatic interactions has been shown to modulate membrane properties in many ways, including their mechanics, dynamics, compositional heterogeneities, and overall stability.[42] This in turn can lead to striking morphological changes, for example, the coiling instability of membrane tubes that can be induced by the hydrophobic anchoring of flexible polymers.[43,44] Therefore, complexation of macromolecules with lipid membranes is an intricate and important problem worthy of further investigation.

Biological Implications. The observations and interpretations we have reported here may have relevance to several physiological processes. First, while the phase separation to induce spatial localization of CL-rich domains within a single vesicle was used here as a convenient experimental tool to simultaneously monitor and compare the behavior of different membrane compositions interacting with cyt *c* under identical experimental conditions, these two coexisting liquid phases in our model GUVs are thought to mimic the structures of natural in vivo membrane heterogeneities driven by lipid−lipid interactions.[45] The L_o phase is assumed to have properties similar to those of nanoscale in vivo domains that are temporally and spatially dynamic, and rich in cholesterol and saturated lipids, often referred to as lipid "rafts", while the L_d phase is thought to mimic the structure of the surrounding "non-raft" membrane environment. Because we observe that CL is largely excluded from the L_o domains due to its highly unsaturated hydrocarbon tails, the CL of native mitochondria are also highly likely to be excluded from any "raft"-like domains. However, the existence of compositional heterogeneities of this sort in the inner mitochondrial membrane is uncertain due to the low cholesterol composition in this membrane and its perceived necessity in forming these domains.[7] On the other hand, considerable amounts of CL are known to transfer to the outer mitochondrial membrane during apoptosis, particularly at intermembrane contact sites:[46] the outer mitochondrial membranes contain a higher cholesterol composition, making "raft" domains more likely to perform significant functions. Indeed, the specific association between cyt *c* and CL that has relocated to the outer mitochondrial membrane may perform a significant role in its escape into the cytosol during apoptosis, for example, in promoting its transport across the membrane. Asymmetric distributions of CL within this outer membrane, which could result from such heterogeneities, would infer the presence of regions of membrane with higher CL concentrations than the mean that could be important for processes that require the cooperative activity of many CL and/or cyt *c* molecules.

Our results may also have significance in understanding the forces and interactions that create and stabilize the structural morphologies of mitochondrial membranes. High curvature and folding is observed in the formation of the cristae of the inner mitochondrial membrane. The folded inner membrane provides a larger surface area for the complexes of the electron transport chain to produce ATP, the energy source that fuels the vital molecular machinery for the survival of living organisms. It is plausible that the relatively high concentrations of cyt *c* in the intermembrane space play a role in the formation and stabilization of these long, narrow folded structures by mechanisms analogous to those that cause the folding of synthetic CL-containing membranes that we report here. The electrostatic attractive interaction induced between two anionic CL-containing membranes by intermediary polycationic cyt *c* proteins could stabilize the narrow width (∼20 nm[15]) of the cristae folds because bare model inner mitochondrial membranes (without bound proteins such as cyt *c*) experience repulsive electrostatic interactions.[47] Therefore, our observations pose an interesting physiological question: is the mitochondrial cristae remodelling, observed in the early stages of apoptosis, a cause or an effect of cyt *c* release into the cytosol?

Other physical explanations for the formation and stability of mitochondrial cristae have been proposed on the basis of experimental observation or theoretical considerations.[48,49] Khalifat et al. create a local pH gradient on the surface of CL-containing GUVS by microinjection of HCl near the outer membrane surface.[48] They observed the formation of tubular invaginations caused by the areal condensation of the outer monolayer due to charge neutralization of the CL headgroups by the protons. The authors formulate a simple geometric model based upon the areal contraction of the outer monolayer and maintaining a constant encapsulated volume of the vesicle to predict the width and length of invaginations and discuss the morphological similarities of their observations to the cristae of the mitochondria. Ponnuswamy et al. formulate a thermodynamic model for the radius of mitochondrial cristae tubules in a mixed PE/PC membrane by considering the curvature elastic energy balanced by an osmotic pressure difference between the mitochondrial matrix and the intermembrane space.[49] The authors note that their model predicts that the tubules are unstable and that additional mechanisms would be required to stabilize them; on the basis of the experimental observations reported here, an energetic contribution due to the electrostatic attraction induced between apposing leaflets of the inner mitochondrial membrane by the cyt *c* in the cristae is a possible mechanism by which these invaginations are stabilized.

CONCLUSIONS

We have engineered synthetic lipid membranes with an asymmetric distribution of CL to investigate differential, composition-specific morphology changes within these vesicles upon addition of cyt *c*. This novel experimental design provides an in-built control experiment that allows simultaneous monitoring of CL-rich and CL-depleted membranes under identical experimental conditions. Cyt *c* is observed to induce budding and collapse of the CL-rich domains. We conclude that this phase extrusion is a nonequilibrium phenomenon driven by nonspecific electrostatic interactions between the anionic membrane domains and the polycationic globular proteins that provokes membrane buckling and subsequent aggregation between different segments of the same membrane. These direct single vesicle observations of the CL−cyt *c* interaction offer compelling insight into their role and function in the mitochondria of the cell, in particular, stabilization of mitochondrial cristae and assisting the escape of cyt *c* into the cytosol during apoptosis.

ASSOCIATED CONTENT

Supporting Information. Two additional figures showing control experiments with protein/polymer additives that did not induce domain collapse (S1) and experiments conducted at

different ionic strength (S2). Time-lapse videos of morphology changes in GUVs induced by cyt *c* or PAMAM G3. This material is available free of charge via the Internet at http://pubs.acs.org.

AUTHOR INFORMATION

Corresponding Author

*Tel.: (203) 432-4220 (T.K.V.); (609) 258-3593 (J.T.G.). Fax: (203) 432-0358 (T.K.V.); (609) 258-0348 (J.T.G.). E-mail: kyle.vanderlick@yale.edu (T.K.V.); jtgroves@princeton.edu (J.T.G.).

Present Addresses

[§]Centre for Molecular Nanoscience, School of Chemistry, University of Leeds, Leeds LS2 9JT, United Kingdom.

ACKNOWLEDGMENT

We thank Dr. Jia Su for informative discussions, Dr. John Eng for support on the mass spectroscopy, and Dr. Joseph Goodhouse for technical support for the Princeton confocal microscope core facility. We gratefully acknowledge the support of Eli Lilly (to C.L.B.) and the National Institutes of Health (2R37 GM036298, MERIT Award to J.T.G.).

REFERENCES

(1) Martin, W. *Proc. R. Soc. London, Ser. B* **1999**, *266*, 1387–1395.
(2) Schapira, A. H. V. *Lancet* **2006**, *368*, 70–82.
(3) Frey, T. G.; Mannella, C. A. *Trends Biochem. Sci.* **2000**, *25*, 319–324.
(4) Schlame, M. *J. Lipid Res.* **2008**, *49*, 1607–1620.
(5) van Beek-Harmsen, B. J.; van der Laarse, W. J. *J. Histochem. Cytochem.* **2005**, *53*, 803–807.
(6) Ow, Y. L. P.; Green, D. R.; Hao, Z.; Mak, T. W. *Nat. Rev. Mol. Cell Biol.* **2008**, *9*, 532–542.
(7) Ardail, D.; Privat, J. P.; Egretcharlier, M.; Levrat, C.; Lerme, F.; Louisot, P. *J. Biol. Chem.* **1990**, *265*, 18797–18802.
(8) Heimburg, T.; Marsh, D. *Biophys. J.* **1995**, *68*, 536–546.
(9) Tuominen, E. K. J.; Wallace, C. J. A.; Kinnunen, P. K. J. *J. Biol. Chem.* **2002**, *277*, 8822–8826.
(10) Cortese, J. D.; Voglino, A. L.; Hackenbrock, C. R. *Biochemistry* **1998**, *37*, 6402–6409.
(11) Balakrishnan, G.; Hu, Y.; Oyerinde, O. F.; Su, J.; Groves, J. T.; Spiro, T. G. *J. Am. Chem. Soc.* **2007**, *129*, 504–505.
(12) Basova, L. V.; Kurnikov, I. V.; Wang, L.; Ritov, V. B.; Belikova, N. A.; Vlasova, I. I.; Pacheco, A. A.; Winnica, D. E.; Peterson, J.; Bayir, H.; Waldeck, D. H.; Kagan, V. E. *Biochemistry* **2007**, *46*, 3423–3434.
(13) Su, J.; Groves, J. T. *Inorg. Chem.* **2010**, *49*, 6317–6329.
(14) Kagan, V. E.; Tyurin, V. A.; Jiang, J. F.; Tyurina, Y. Y.; Ritov, V. B.; Amoscato, A. A.; Osipov, A. N.; Belikova, N. A.; Kapralov, A. A.; Kini, V.; Vlasova, I. I.; Zhao, Q.; Zou, M. M.; Di, P.; Svistunenko, D. A.; Kurnikov, I. V.; Borisenko, G. G. *Nat. Chem. Biol.* **2005**, *1*, 223–232.
(15) Sun, M. G.; Williams, J.; Munoz-Pinedo, C.; Perkins, G. A.; Brown, J. M.; Ellisman, M. H.; Green, D. R.; Frey, T. G. *Nat. Cell Biol.* **2007**, *9*, 1057–U21.
(16) Kagan, V. E.; Bayir, A.; Bayir, H.; Stoyanovsky, D.; Borisenko, G. G.; Tyurina, Y. Y.; Wipf, P.; Atkinson, J.; Greenberger, J. S.; Chapkin, R. S.; Belikova, N. A. *Mol. Nutr. Food Res.* **2009**, *53*, 104–114.
(17) Perroud, T. D.; Bokoch, M. P.; Zare, R. N. *Proc. Natl. Acad. Sci. U.S.A.* **2005**, *102*, 17570–17575.
(18) Veatch, S. L.; Keller, S. L. *Biophys. J.* **2003**, *85*, 3074–3083.
(19) Sengupta, P.; Hammond, A.; Holowka, D.; Baird, B. *Biochim. Biophys. Acta, Biomembr.* **2008**, *1778*, 20–32.
(20) Tanford, C.; Roxby, R. *Biochemistry* **1972**, *11*, 2192.
(21) Uversky, V. N. *J. Neurochem.* **2007**, *103*, 17–37.
(22) Bronich, T. K.; Solomatin, S. V.; Yaroslavov, A. A.; Eisenberg, A.; Kabanov, V. A.; Kabanov, A. V. *Langmuir* **2000**, *16*, 4877–4881.
(23) Yaroslavov, A. A.; Rakhnyanskaya, A. A.; Yaroslavova, E. G.; Efimova, A. A.; Menger, F. M. *Adv. Colloid Interface Sci.* **2008**, *142*, 43–52.
(24) Ilett, S. M.; Orrock, A.; Poon, W. C. K.; Pusey, P. N. *Phys. Rev. E* **1995**, *51*, 1344–1352.
(25) Gelbart, W. M.; Bruinsma, R. F.; Pincus, P. A.; Parsegian, V. A. *Phys. Today* **2000**, *53*, 38–44.
(26) Cametti, C. *Chem. Phys. Lipids* **2008**, *155*, 63–73.
(27) DeMeulenaer, B.; VanderMeeren, P.; DeCuyper, M.; Vanderdeelen, J.; Baert, L. *J. Colloid Interface Sci.* **1997**, *189*, 254–258.
(28) Zimmerberg, J.; Kozlov, M. M. *Nat. Rev. Mol. Cell Biol.* **2006**, *7*, 9–19.
(29) Zidovska, A.; Ewert, K. K.; Quispe, J.; Carragher, B.; Potter, C. S.; Safinya, C. R.; Block *Langmuir* **2009**, *25*, 2979–2985.
(30) Bashkirov, P. V.; Akimov, S. A.; Evseev, A. I.; Schmid, S. L.; Zimmerberg, J.; Frolov, V. A. *Cell* **2008**, *135*, 1276–1286.
(31) Evans, E.; Rawicz, W. *Phys. Rev. Lett.* **1990**, *64*, 2094–2097.
(32) Helfrich, W.; Servuss, R. M. *Nuovo Cimento Soc. Ital. Fis., D* **1984**, *3*, 137–151.
(33) Marsh, D. *Chem. Phys. Lipids* **2006**, *144*, 146–159.
(34) Abraham, F. F.; Kardar, M. *Science* **1991**, *252*, 419–422.
(35) Pocivavsek, L.; Dellsy, R.; Kern, A.; Johnson, S.; Lin, B. H.; Lee, K. Y. C.; Cerda, E. *Science* **2008**, *320*, 912–916.
(36) Heimburg, T.; Angerstein, B.; Marsh, D. *Biophys. J.* **1999**, *76*, 2575–2586.
(37) McLaughlin, S.; Murray, D. *Nature* **2005**, *438*, 605–611.
(38) Gorbenko, G. P.; Trusova, V. M.; Molotkovsky, J. G.; Kinnunen, P. K. J. *Biochim. Biophys. Acta, Biomembr.* **2009**, *1788*, 1358–1365.
(39) Seddon, J. M. *Biochim. Biophys. Acta* **1990**, *1031*, 1–69.
(40) Dekruijff, B.; Cullis, P. R. *Biochim. Biophys. Acta* **1980**, *602*, 477–490.
(41) Seddon, J. M.; Kaye, R. D.; Marsh, D. *Biochim. Biophys. Acta* **1983**, *734*, 347–352.
(42) Tribet, C.; Vial, F. *Soft Matter* **2008**, *4*, 68–81.
(43) Frette, V.; Tsafrir, I.; Guedeau-Boudeville, M. A.; Jullien, L.; Kandel, D.; Stavans, J. *Phys. Rev. Lett.* **1999**, *83*, 2465–2468.
(44) Tsafrir, I.; Guedeau-Boudeville, M. A.; Kandel, D.; Stavans, J. *Phys. Rev. E* **2001**, *63*, 031603.
(45) Hancock, J. F. *Nat. Rev. Mol. Cell Biol.* **2006**, *7*, 456–462.
(46) Kagan, V. E.; Bayir, H. A.; Belikova, N. A.; Kapralov, O.; Tyurina, Y. Y.; Tyurin, V. A.; Jiang, J. F.; Stoyanovsky, D. A.; Wipf, P.; Kochanek, P. M.; Greenberger, J. S.; Pitt, B.; Shvedova, A. A.; Borisenko, G. *Free Radical Biol. Med.* **2009**, *46*, 1439–1453.
(47) Nichols-Smith, S.; Kuhl, T. *Colloids Surf., B* **2005**, *41*, 121–127.
(48) Khalifat, N.; Puff, N.; Bonneau, S.; Fournier, J. B.; Angelova, M. I. *Biophys. J.* **2008**, *95*, 4924–4933.
(49) Ponnuswamy, A.; Nulton, J.; Mahaffy, J. M.; Salamon, P.; Frey, T. G.; Baljon, A. R. C. *Phys. Biol.* **2005**, *2*, 73–79.